ACS NANO

www.acsnano.org

ARTICLE

On-Surface Site-Selective Cyclization of Corrole Radicals

Stefano Tebi,[†,⊥] Mateusz Paszkiewicz,[‡,⊥] Hazem Aldahhak,[§,⊥] Francesco Allegretti,[‡] Sabrina Gonglach,[∥] Michael Haas,[∥] Mario Waser,[∥] Peter S. Deimel,[‡] Pablo Casado Aguilar,[‡] Yi-Qi Zhang,[‡] Anthoula C. Papageorgiou,[‡] David A. Duncan,[‡] Johannes V. Barth,[‡] Wolf G. Schmidt,[§] Reinhold Koch,[†] Uwe Gerstmann,[*,§] Eva Rauls,[*,§] Florian Klappenberger,[*,‡] Wolfgang Schöfberger,[*,∥] and Stefan Müllegger[*,†]

[†]Institute of Semiconductor and Solid State Physics and [∥]Institute of Organic Chemistry, Johannes Kepler University, Altenberger Straße 69, 4040 Linz, Austria

[‡]Physics Department E20, Technical University of Munich, James-Franck Straße 1, 85748 Garching, Germany

[§]Physics Department, Paderborn University, Warburger Straße 100, 33098 Paderborn, Germany

Supporting Information

ABSTRACT: **Radical cyclization is among the most powerful and versatile reactions for constructing mono- and polycyclic systems, but has, to date, remained unexplored in the context of on-surface synthesis. We report the controlled on-surface synthesis of stable corrole radicals on Ag(111) *via* site-specific dehydrogenation of a pyrrole N−H bond in the 5,10,15-tris(pentafluoro-phenyl)-corrole triggered by annealing at 330 K under ultrahigh-vacuum conditions. We reveal a thermally induced regioselective cyclization reaction mediated by a radical cascade and resolve the reaction mechanism of the pertaining cyclodefluorination reaction at the single-molecule level. *Via* intramolecularly resolved probing of the radical-related Kondo signature, we achieve real space visualization of the distribution of the unpaired electron density over specific sites within the corrole radical. Annealing to 550 K initiates intermolecular coupling reactions, producing an extended π-conjugated corrole system.**

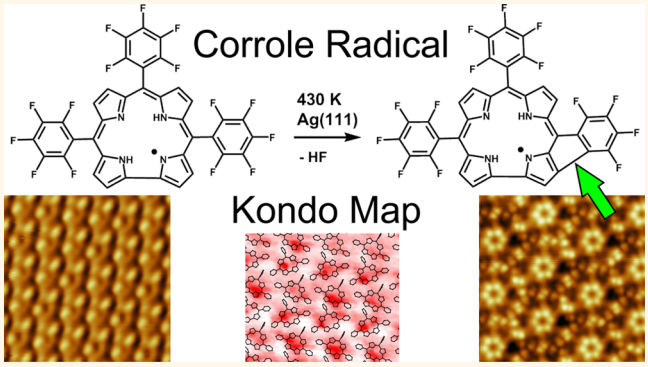

KEYWORDS: *corrole, radical cascade reactions, regioselectivity, cyclization, defluorination, surface, network*

Tetrapyrrolic macrocycles are well-established building blocks of interfacial covalent architectures for heterogeneous catalysis,[1−8] and recent on-surface synthetic routes enable the fabrication of architectures with high stability and atomic precession.[9−13] Existing on-surface synthetic routes include Ullmann coupling,[14] imidization,[15,16] cross-linking of porphyrins,[17,18] cyclodehydrogenation of cyclohexa-*o*-*p*-*o*-*p*-*o*-*p*-phenylene to tribenzo[*a*,*g*,*m*]coronene,[19] and oligomerization of heterocyclic carbenes[20] as well as polyimines.[21] In contrast to these ionic or concerted reactions, radical cascade reactions proceed through two or more consecutive steps, mediated by the radical's unpaired electron. Radical cascades provide a complementary and scientifically appealing strategy, due to their undeniable benefits,[22−27] including extraordinarily high atom economy,[28] enabling time-, labor-, and resource-efficient management, and reduced waste generation. Thus, radical cascade reactions are a promising route toward "green chemistry".[29] To date, however, site-selective radical cascades are hardly explored in the context of surface-confined synthesis. Here we show the example directed to covalently couple 18-π-electron macrocyclic precursors on surfaces *via* a radical cascade that allows the preparation of two-dimensional molecular architectures (with extended π-aromatic character) which cannot be synthesized in solution.

We clarify the on-surface reaction mechanism of defluorinative cyclization reaction of the 5,10,15-tris-(pentafluorophenyl)-corrole (H_3TpFPC, Figure 1) on the Ag(111) surface. By combining scanning tunnelling microscopy as a high-resolution local probe, element-specific X-ray spectroscopy techniques, and density functional theory (DFT) calculations, we reveal a rich covalent chemistry at the single-molecule level under ultrahigh-vacuum conditions.

Received: February 3, 2017
Accepted: February 17, 2017
Published: February 17, 2017

DOI: 10.1021/acsnano.7b00766
ACS Nano 2017, 11, 3383−3391

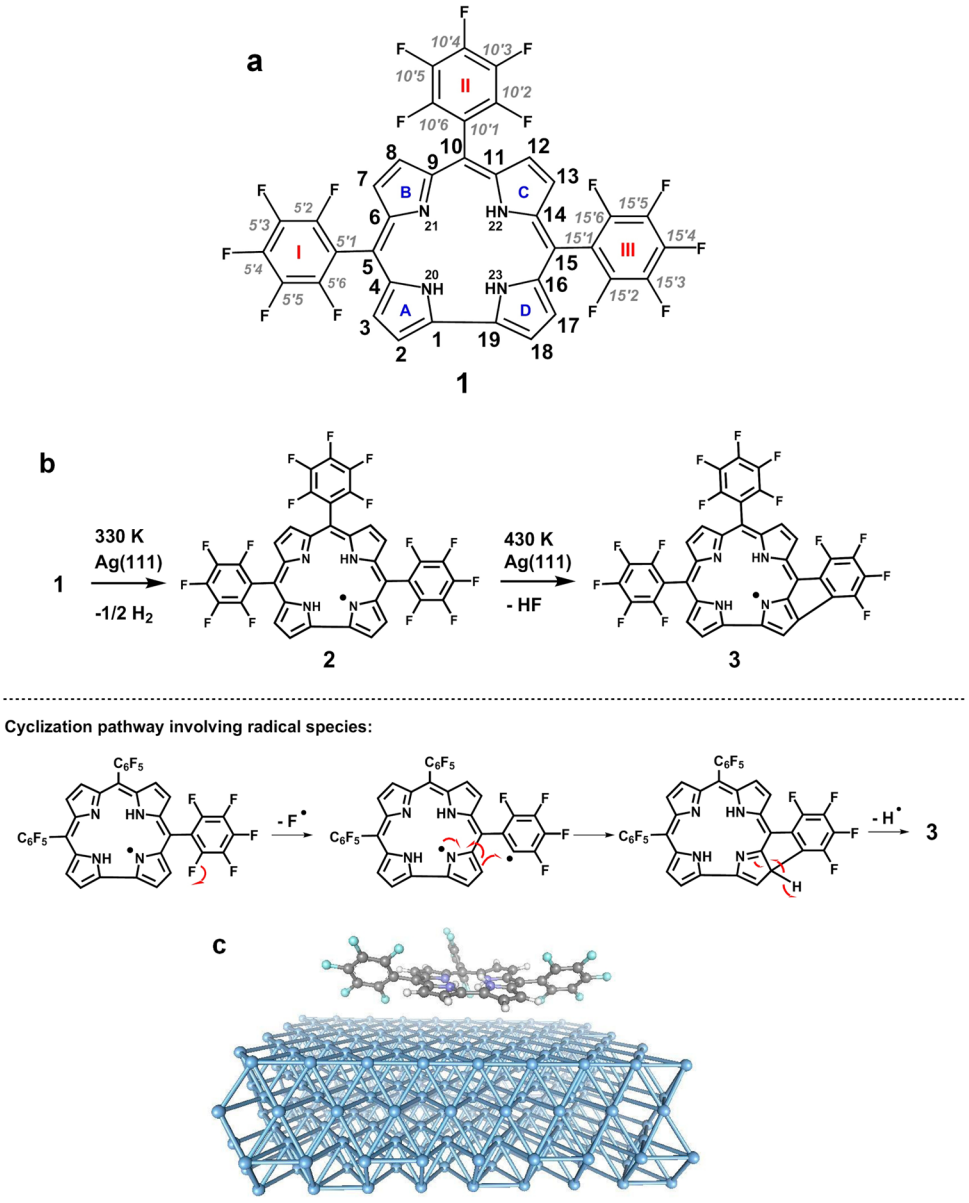

Figure 1. (a) Chemical representation of the H_3TpFPC molecule 1 (5,10,15-tris(pentafluorophenyl)-corrole); (b) the thermally induced radical cascade reaction on Ag(111); and (c) the side-view of the adsorption geometry of an isolated corrole at the Ag(111) surface. The C atoms forming the tetrapyrrole macrocycle are labeled 1−19; the N atoms of the tetrapyrrole macrocycle are labeled 20−23; individual pyrrole groups are labeled A−D;[30] pentafluorophenyl ($-C_6F_5$) groups in *meso*-position 5, 10, and 15 are labeled I, II and III, respectively; C atoms of $-C_6F_5$ groups are labeled by two numbers, indicating, first, the *meso*-position, and, second, the atom number of the phenyl (1−6).

We demonstrate that at 330 K, the Ag(111) surface triggers the selective homolytic cleavage of a pyrrolic N−H bond. The dehydrogenation reaction generates a stable radical species exhibiting electron spin (magnetization density) at specific intramolecular positions. Starting at an intriguingly moderate temperature close to 400 K, a radical cascade initiates a site-selective defluorination reaction resulting in an intramolecular cyclization between macrocycle and *meso*-substituent. Further thermal activation causes substantial fluorine abstraction and intermolecular coupling, forming irregular but highly conjugated corrinoid networks. Our synthesis protocols employing defluorination/dehalogenation reactions as elementary steps for the construction of corrinoid building blocks and corrinoid architectures leading to unprecedented catalytically active hybrid materials.

RESULTS AND DISCUSSION

Corrole Radical on Ag(111). Silver was selected as the substrate material of choice, because of its high relevance as electrode material for heterogeneous catalysis. We have investigated the fluorinated free-base corrole, H_3TpFPC (Figure 1a), adsorbed on single-crystal Ag(111) under ultrahigh-vacuum, and Figure 2a shows a representative STM image of a compact monolayer of H_3TpFPC on Ag(111) at 200 K[31] and subsequently annealed to 330 K. The STM image reveals a well-ordered arrangement of molecules[32] similar to free-base corroles on Au(111)[33] as well as metal corroles.[34] After deposition at 150 K, temperature-programmed desorption (TPD) reveals desorption of molecular H_2 at around room temperature (300 K, Figure 2b, curve H_2). Since direct formation of molecular hydrogen is unlikely,[35] the peak

DOI: 10.1021/acsnano.7b00766
ACS Nano 2017, 11, 3383−3391

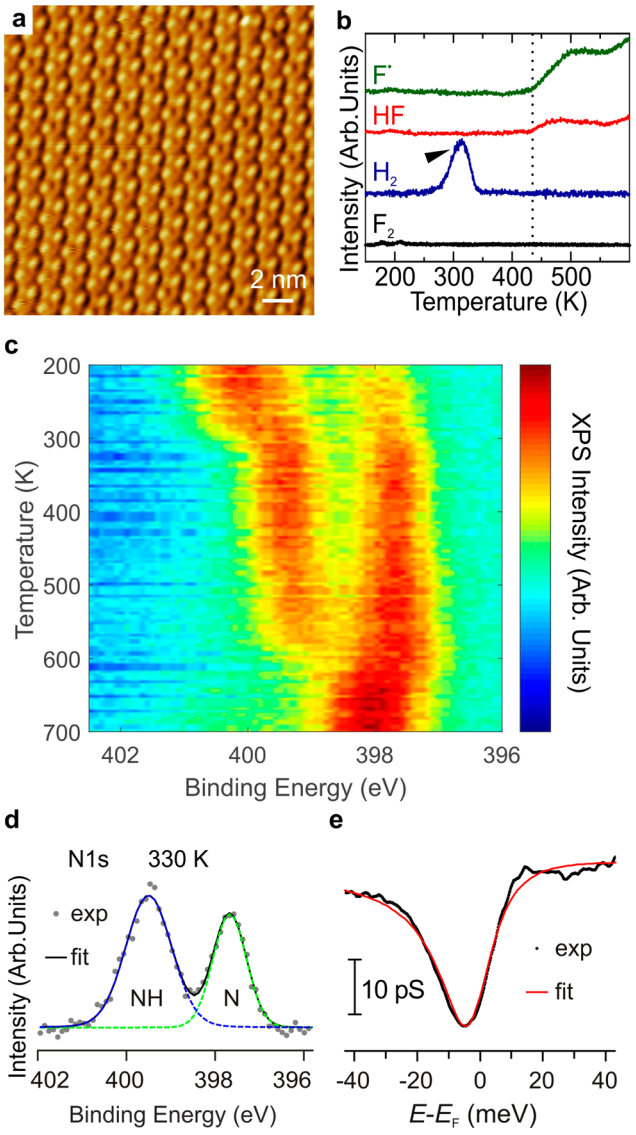

Figure 2. Corrole radical formation on Ag(111) at 330 K. (a) Representative STM image (+1 V, 100 pA, 20 × 20 nm^2, 5 K) of an ordered monolayer of H_2TpFPC$^\bullet$ (species 2) molecules adsorbed on Ag(111) after annealing to 330 K. (b) TPD spectra of H_3TpFPC grown on Ag(111) at 150 K and linearly heated to 600 K with a heating rate of 0.25 K/s; the curves represent, from top to bottom, the desorption from the surface of atomic F$^\bullet$, HF, H_2, and F_2 detected by mass spectrometry. (c) Temperature-programmed N 1s XPS measurement of H_3TpFPC on Ag(111) between 200 and 700 K with a heating rate of 0.1 K/s. (d) N 1s XPS spectrum of the H_2TpFPC$^\bullet$ corrole radical; the two peaks are attributed to NH and N (please note the decrease of binding energies from 400 and 398 eV to 399.4 and 397.8 eV due the formation of H_2TpFPC$^\bullet$ corrole radical species. (e) Scanning tunneling conductance (dI/dV) spectrum of the H_2TpFPC$^\bullet$ corrole radical on Ag(111) obtained by STM; the experimental curve (black) represents the average of 10 independent measurements performed over different individual corrole molecules within the monolayer and is numerically fitted (red) by a Fano line shape[42] with parameters q = 0.18; E_K = 2.8; Γ = 10.2.

indicates the abstraction of H atoms from the corrole molecules. Correspondingly, in temperature-programmed N 1s XPS (Figure 2c), a dramatic change is observed over a similar temperature range. Below 300 K, similar to multilayer reference systems,[31] the N 1s XP spectrum consists of two peaks at a binding energy of 400 and 398 eV with an intensity ratio of almost 3:1, assigned to the three aminic −NH nitrogen atoms (N20, N22, N23) and the iminic −N= atom (N21) (Figure 1), respectively. Between 300 and 400 K, the N−H and the −N= peak shifts in binding energy to 399.4 and 397.8 eV and become almost equivalent in intensity (Figure 2c,d) indicating the cleavage of one of the N−H bonds, not observed for multilayer samples. According to our DFT calculation, it is the H atom at N23 (Figure 1) that is preferentially cleaved in order to maximize the distance of the remaining two H atoms. The cleaved H atom is then observed to recombine on the surface and desorb in the aforementioned H_2 TPD (a well-known process on noble metal surfaces).[36] To further clarify whether the H abstraction forms a corrole radical or corrole anion, we have applied an STM tip as local probe, capable of identifying radical species at a submolecular level based on the surface Kondo effect.[37−39] A characteristic minimum of the tunnel conductance, dI/dV, in a narrow energy range close to the Fermi energy is detected by STM locally at the individual corrole molecules (Figure 2e). This so-called Kondo signature (absent over the bare Ag(111) substrate) provides evidence for the presence of unpaired electron (spin) density,[39] thus revealing the radical nature of the surface-adsorbed corrole on Ag(111) at 330 K. We denote the corrole radical as H_2TpFPC$^\bullet$ (species **2**, see Figure 1). Note that the existence of a stable corrole radical species, in general, has been revealed only very recently in liquid phase by the Bröring group.[40] The differential-conductance minimum lies slightly below the Fermi energy (close to −3.4 mV) indicating particle-hole asymmetry[39,41] due to a partial negative charge transfer from the Ag substrate to the H_2TpFPC$^\bullet$ radical. This experimental finding is corroborated by our first-principles calculations yielding a partial charge transfer from the metallic surface to the molecule of approximately −0.2 e (where e is the elementary charge). This partial charge transfer explains also the reduced binding energies of aminic −NH and iminic =N− nitrogen atoms in the N 1s XPS spectra (Figure 2c,d).

We have successfully imaged the spatial distribution of the radical electron spin density within the individual H_2TpFPC$^\bullet$ molecules with subnanometer resolution by STM. Figure 3a,b presents representative STM images of the corrole monolayer, showing the topographic contrast (a) and the radical signal (b), *i.e.*, the height of the Kondo signal, measured over the same image frame with submolecular resolution.

We identify the relative positions of the individual corrole molecules in the monolayer with high precision, based on a structural analysis of the arrangement of molecules previously demonstrated by some of the present authors.[32] The positions of the corrole molecules are illustrated in Figure 3b as an overlaid idealized, highly periodic structure model. Apparently, the unpaired electron is always observed at the macrocycle. For the preferential structure **2a**, we calculate strong electron spin density centered at the lower right half of the macrocycle (defined by an imaginary line through the two remaining aminic −NH atoms), as illustrated in Figure 3c. Nevertheless, having in mind a possible thermal movement of the central H atom, an alternative structure **2b** cannot be conclusively excluded. It shows a slightly different distribution of the spin density (Figure 3c), thereby providing a reasonable explanation for the fluctuations visible in the experimental Kondo image. A similar nonuniform distribution of the unpaired electron

DOI: 10.1021/acsnano.7b00766
ACS Nano 2017, 11, 3383−3391

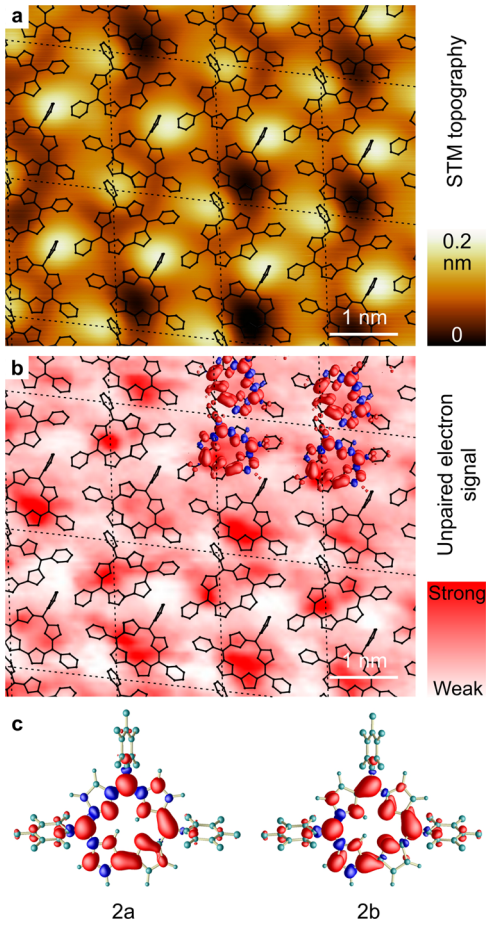

Figure 3. Real space visualization of the H_2TpFPC$^\bullet$ corrole radical spin density translocation. (a) Topographic STM image of H_2TpFPC$^\bullet$ on Ag(111); +0.3 V, 100 pA, 6 × 5 nm^2). (b) Same image frame as in (a) showing the spatial distribution of the electron spin density (Kondo signal obtained from the magnitude of the local tunnel conductance at −3 mV sample bias as recorded experimentally by scanning conductance spectroscopy; average of 15 consecutive frames, equivalent to 15 h of total measuring time). (c) DFT-calculated distribution of the unpaired electron spin density $m = n_\uparrow(\vec{r}) - n_\downarrow(\vec{r})$, where $m > 0$ ($m < 0$) is plotted in red (blue), given for the preferential structure 2a and an alternative 2b.

density was shown by Komeda and Wu *et al.* in a copper corrole derivative on Au(111).[43]

We have confirmed the stability of the H_2TpFPC$^\bullet$ species in a temperature range up to about 400 K, based on TPD (Figure 2b) and temperature-programmed N 1s XPS (Figure 2c) data, where no evidence of additional chemical reactions has been found.

Intramolecular Ring Closure. Above 430 K, the existence of an additional reaction, which involves both H and F, is indicated by the detection of F$^\bullet$ and HF in the TPD curves of Figure 2b. Furthermore, the absence of H_2 desorption precludes processes where H and F atoms are abstracted individually through chemisorption onto the surface, followed by recombination and desorption. Thus, the TPD data suggest a reaction where H and F are abstracted in a correlated way forming HF molecules at or near the reacting species.

C 1s XPS measurements above and below the temperature range of this transition reveal further details of this additional reaction step: The C 1s spectrum of the sample annealed at 430 K exhibits an additional shoulder, marked by an arrow (Figure 4b), which is absent at 330 K (Figure 4a). With the help of DFT simulations (Figure 4c), the shoulder can be attributed to a specific C−C bond (ring closure) between one of the C_6F_5 groups and the macrocycle, like that formed between C atoms 17 and 15′2; the respective ring-closed species (**3**) is illustrated in Figures 1 and S1. Figure 1C shows the cyclization pathway involving correlated radical and HF formation; notice that the individual H and F abstraction reactions occur at short enough time scales (ps) to enable highly efficient recombination and desorption of HF.

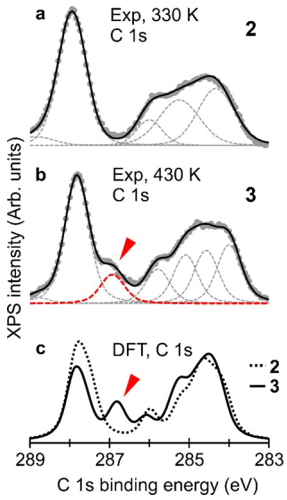

Figure 4. Formation of ring-closed corrole species on Ag(111) close to 430 K *via* cyclodefluorination reaction. (a, b) Experimental C 1s XPS data of free-base corrole on Ag(111) obtained after annealing at (a) 330 K and (b) 430 K; respective chemical schemes are illustrated in Figure S1; the arrow marks C−F signature of $-C_6F_4$ group, indicating ring closure (see text). (c) DFT simulation of the C 1s XPS spectrum of the H_2TpFPC$^\bullet$ radical (dotted line, species 2) and ring-closed corrole (solid line, species 3) on Ag(111).

Having in mind its essential role for stabilizing the adsorption geometry (Figure 1), it is rather unlikely that the central strongly tilted C_6F_5 group bound to C10 is involved in an initial ring closure. This is in agreement with our STM and DFT results, discussed below, and represents a certain degree of regioselectivity of the ring closure. However, alternative structures with the additional C−C bond between C atoms 3 and 5′6 or even C7−C5′2 and C13−C15′6 are possible and result in energetically nearly equivalent structures with almost identical XPS signals (Figure S5). In other words, despite being a clear indicator for a cyclization reaction, the shoulder feature in the XPS data is not specific enough to distinguish cyclization occurring at these different possible sites.

Figure 5a,b shows representative experimental STM images of a single isolated H_2TpFPC$^\bullet$ annealed to 330 K (species **2**) and a ring-closed corrole annealed to 430 K species **3**; the individual single molecules have been obtained by STM-based manipulation of densely packed molecular islands.[32] STM reveals the triangle-like topographic appearance of the two species, characteristic of adsorbed corroles,[32,33,44] but with a slightly different shape and symmetry: The image of the ring-closed species **3** exhibits reduced symmetry compared to species **2**.

Notice that a comparison of experimental and DFT-simulated STM images, discussed in the following, indicates a high regioselectivity of the ring-closure reaction: For

DOI: 10.1021/acsnano.7b00766
ACS Nano 2017, 11, 3383−3391

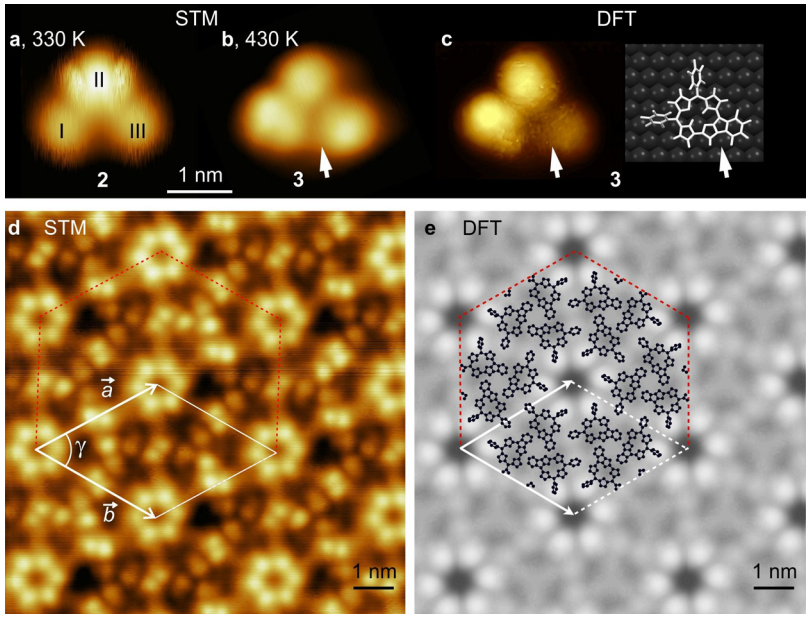

Figure 5. Ring-closed corrole radical. (a, b) Experimental STM images (+1 V, 100 pA, 3 × 3 nm^2, 5K) of single H_2TpFPC$^\bullet$ radicals on Ag(111) after annealing to (a) 330 K (species 2) and (b) to 430 K (ring-closed species 3); labels I−III mark the $-C_6F_5$ groups. (c) DFT-calculated STM image (left) and molecular structure of the ring-closed radical species 3; the arrow marks the position of ring closure (as guide to the eye); compare with (a). (d) Experimental STM image (+0.2 V, 1 nA, 10 × 10 nm^2, 5K) and (e) DFT-calculated STM image of an idealized monolayer of ring-closed corrole 3 after annealing to 430 K; in (d) the regular unit cell is indicated by vectors $|\vec{a}| = |\vec{b}| \approx 3.4$ nm, angle $\gamma = 60°$; in e) the regular molecular arrangement of the monolayer is overlaid, as obtained from DFT optimization.

comparison, Figure 5c shows the calculated STM image (left) of the C17/C15′2 (or equivalently C3/C5′6) ring-closed corroles together with the respective molecular structure model (right) obtained from our first-principles calculations. The agreement between calculation (Figure 5c) and experiment (Figure 5b) is very good. In particular, the low-symmetric appearance of species **3** is well explained by the ring closure causing an increased flattening of the molecular structure at the position of the respective C−C bond (marked by an arrow as guide to the eye). Our STM results reveal only such ring-closed corrole species with topographic appearance similar to Figure 5b, indicating regioselectivity of ring closure at position C17/C15′2 (or equivalently C3/C5′6).

Intriguingly, the ring-closed radical species **3** forms a highly symmetric regular monolayer structure on Ag(111) at 430 K, as illustrated by the STM image of Figure 5d. The approximately hexagonal lattice is described by cell vectors $\vec{a}$ and $\vec{b}$. With our DFT simulations we have successfully resolved the molecular packing motif of the individual corrole molecules within this monolayer structure (*i.e.*, the molecular basis), as illustrated in Figure 5e. The structure contains six singly ring-closed molecules per unit cell. Notice that the simulated structure is based on an idealized model containing only one ring-closed conformer. In comparison, the experimental STM image of Figure 5d deviates locally from such strict periodicity of the ring-closure positions. Compared to the monolayer of species **2**, whose two-dimensional space group has an apparent *P*1 symmetry, the hexagonal monolayer of the ring-closed species **3** exhibits an increased pseudosymmetry of approximately *P*6. This apparently counterintuitive observation can be explained as follows: As mentioned above, initial ring closure at the central C_6F_5 groups, bound to C10, is therefore unlikely. The remaining possibilities for species **3** are isomers, which differ only slightly by the position of the ring closure and by the positions of the H atoms in the center of the macrocycle, resulting in an inherently similar shape. A packing motif consisting of neighboring tilted and flattened side groups allows dense aggregation. Simultaneously, the central C_6F_5 groups, bound to C10, are forced to be grouped together in a hexagonal arrangement, accompanied by a further enlarged tilt away from the substrate to maximize the intermolecular F−F distance. As the individual corroles exhibit a pseudo-two-fold symmetry and are adsorbed on a three-fold symmetric substrate, the origin of the pseudo-six-fold symmetric monolayer becomes quite clear.

Further annealing of the sample causes further desorption of H and F, which starts close to 440 K as indicated by TPD (see Figure 2b), indicating additional dehydrogenation and defluorination processes. The additional dehydrogenation process at temperatures above 430 K is corroborated by the N 1s XPS measurements of Figures 2c and S2, evidencing a strong decrease of the pyrrolic N−H signal intensity from 450 to 550 K. By scanning tunnelling spectroscopy, we were able to obtain Kondo signals from individual corrole radicals up to at least 460 K (Figure 3b,c), suggesting the existence of unpaired electron spin density even in the ring-closed species (cf. Figure 2c). These results indicate that a radical cascade is induced and further intramolecular ring-closure reactions occur between the pyrrole carbons and the C_6F_5 groups. The temperature range of the additional ring closures spans from approximately 430 to 550 K, as indicated by the TPD curves of Figure 2b. Already at 460 K, the structure of the monolayer is found to be highly disordered (Figure S3), in striking contrast to the regular structure at 430 K, indicating a mixture of different species as well as first intermolecular linkages (Figure S4).

Elevated-Temperature Structures of Corrole. With an increasing amount of ring closures, the molecular species appear to become more and more flattened. Thereby the intermolecular distance is considerably reduced, enabling further intermolecular linkages. This scenario is indicated by the strong decrease of the F 1s signal at 700 K (Figure 6a),

DOI: 10.1021/acsnano.7b00766
ACS Nano 2017, 11, 3383−3391

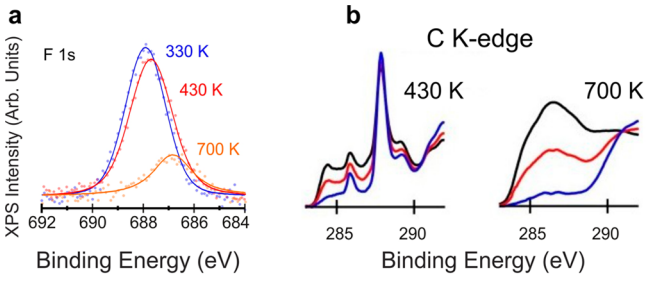

Figure 6. Corrole molecules at elevated temperatures. (a) F 1s photoelectron spectra of corrole radical layer annealed to different temperatures as labeled. (b) Near-edge X-ray-absorption fine-structure measurements on the carbon K-edge of the corrole layer annealed to 430 and 700 K for different values of incidence angle ϕ of 25° (black), 53° (red), and 90° (blue).

which can no longer be explained by ring closures of the individual molecular species. To identify a possible network-like structure of corroles, near-edge X-ray- absorption fine-structure measurements on the carbon K-edge were carried out for the full investigated temperature range (Figure 6b). The angle-dependent spectra after 430 K annealing consist of two sharper peaks at 286 and 288 eV, which originate from π^* resonances related to the fluorinated phenyl rings superposed to a broader structure related to a series of macrocycle-related resonances. With increasing incidence angle ϕ, the macrocycle signal is strongly reduced, while the phenyl resonances remain unchanged. These angle dependences evidence a macrocycle orientation near planar with the surface (~20°) contrasted by significantly tilted phenyl substituents (~50°−60°) consistent with the DFT-optimized geometry of species **3** (Figure 5c). Annealing up to 700 K causes the disordered compact layer to dissolve and the formation of a network-like structure, as shown by the representative STM image of Figure S4 with similar apparent height of 0.14 nm excluding a vertical stacking of molecules.

Interestingly, after 700 K annealing, the angle-dependent carbon K-edge spectra (Figure 6b, right panel) have lost the sharp features and exhibit strong and nearly uniform dichroism throughout the whole π^* range (below 290 eV). Such spectra indicate an overall flattened orientation of the surface-supported corroles, where the originally tilted phenyl rings have been incorporated into a more planarized structure. Similarly, a broad absorption feature is typical for conjugated π-electronic systems such as graphene[45] or nitrogen-doped graphitic carbon networks.[46] In the present case, we expect that the apparent irregular porosity of the structure (see STM image of Figure S4) further increases the broadening. The agreement between the experimental C 1s XPS signatures and the model-based simulations for all investigated temperatures up to 700 K (Figures 4, S1, and S4) is striking, whereby intermolecular binding is shown to start around 500 K (Figure S4) and the formation of a network-like structure is almost completed at 700 K. Our findings, thus, evidence that the corrole character survives such thermal treatment and qualify the network-like structure as a promising starting point for the future fabrication of catalytically active interfaces.

CONCLUSIONS

In summary, we have demonstrated the covalent coupling of molecular corrole precursors on a metallic substrate. It is shown that the Ag(111) surface at 330 K triggers the selective homolytic cleavage of a pyrrolic N−H bond in fluorinated corrole molecules, forming corrole radicals on the surface and initiating radical cascade reactions. We report a temperature protocol for the stepwise synthesis of cyclodefluorinated corroles as well as intermolecularly linked free-base corroles: Surface-adsorbed corrole radicals stable up to 430 K are followed by radical-cascade reactions at elevated temperatures, causing site-selective rearomatization (ring closure) and flattening of the molecular species. Above 550 K, formation of covalently coupled corroles on Ag(111) is revealed. We have clarified the reaction mechanism of dehydrogenation and cyclodefluorination processes at a submolecular (atomic) level, including intramolecular imaging of the spatial distribution of the corrole radical's electron spin. The latter is found to be decisive for the ring-closure reaction. Our work represents a significant step forward toward artificial two-dimensional molecular architectures, which are catalytically active and promise synthetic routes impossible in solution to date. The resulting π-conjugated systems are expected to impact various fields of timely research, including postfossil (alternative) energy sources, energy storage devices, extended π-aromatic systems for energy conversion, as well as artificial systems for water splitting and CO_2 reduction. Combined with well-established *in situ* metalation protocols, a wide range of previously inaccessible covalent materials containing high-valent metal centers come into reach.[47] Thanks to the radical character of the cascade reaction for the underlying corrinoid architectures, all this can be achieved in a kind of "green chemistry", *i.e.*, with extraordinarily atomic precision and economy, enabling time-, labor-, and resource-efficient management of the synthesis.

EXPERIMENTAL SECTION

Materials and Methods. Molecule Synthesis. 5,10,15-tris-(pentafluorophenyl)corrole (H_3TpFPC) was synthesized according to reported procedures,[48] purified by preparative HPLC, and subsequently analyzed by ^{1}H, ^{13}C, and ^{19}F NMR spectroscopy.

Sample Preparation. The Ag(111) substrate was cleaned by several cycles of Ar^+ ion sputtering (600 eV) and thermal annealing (700 K). Samples were prepared by thermal evaporation of the H_3TpFPC molecules from a quartz crucible, kept at 460 K, onto the Ag(111) surface kept at 200 K. Subsequent thermal annealing was performed as described in the text.

Scanning Tunnelling Microscopy and Spectroscopy. The measurements were performed in UHV ($<1 \times 10^{-10}$ mbar) at 5 K, employing electrochemically etched W tips, deoxidized by annealing at $T > 1070$ K in UHV. The tip quality was verified by measuring the well-known surface state of the clean Ag(111) at −70 mV.[49] STM images were analyzed using the program WSxM.[50]

X-ray Photoelectron Spectroscopy (XPS). The measurements were performed at room temperature in normal emission geometry at the BESSY II synchrotron in Berlin, using the HE-SGM beamline (1500 l/mm monochromator grating; 200 μm slit width; Scienta R3000 hemispherical analyzer; base pressure 1×10^{-9} mbar and the UE56−2 PGM-2 undulator beamline (movable end station with a base pressure of 8×10^{-11} mbar; SPECS Phoibos 100 CCD analyzer; 10 μm exit slits after monochromator; entrance slits after undulator aperture were appropriately closed to reduce photon flux and minimize beam damage). Sample position was frequently changed between different spectra to avoid artifacts due to radiation damage. The fast XPS data were recorded in single bunch mode to ensure negligibe beam damage throughout the extended acquisition time. The C 1s spectra were acquired with a pass energy of 10 eV and N 1s and F 1s with 20 eV. The photon energy $h\nu$ was adjusted such that the kinetic energy of the electrons was approximately 150 eV (C 1s, 435 eV; N 1s, 550 eV, F 1s, 850 eV). The binding energy scale was calibrated against

DOI: 10.1021/acsnano.7b00766
ACS Nano 2017, 11, 3383−3391

the Ag $3d_{5/2}$ peak (368.3 eV) or the Fermi edge (0 eV) of the substrate. The spectra were fitted with peaks exhibiting a Voigt line shape after a Shirley (C 1s), linear (F 1s), or polynomial background of fifth-order (N 1s) background subtraction.

Near-Edge X-ray-Absorption Fine-Structure. The spectra were recorded at the HE-SGM beamline, with a monochromator grating of 1500 l/mm and slit widths of 200 μm, in partial electron yield mode at a retarding voltage of −150 V and −250 eV for the C and N K-edge, respectively. The spectra were measured at different incident angles ϕ (25°, 53°, 90°) formed by the E-vector of the incident light (90% linear polarization) with respect to the surface normal. To improve the signal-to-noise ratio, several spectra were collected, and the average is presented in this work. After subtraction of the signal of the bare crystal from the raw data, the measured spectra were normalized to an edge jump of one.

Temperature-Programmed Desorption (TPD). The measurements were performed with a custom-built UHV chamber previously mounted at the UE-56-2 PGM-2 beamline. The base pressure was improved to 3×10^{-11} mbar during the measurements, to reduce the background pressure of H_2 close to the detection limit of the mass spectrometer. A liquid nitrogen cooled quadrupole mass spectrometer equipped with a Feulner cup was employed, which can be brought near to the sample to within a few mm. The heating rate was controlled by a proportional-integral-derivative controller. The cleanliness of the Ag(111) substrate and the coverage and chemical state of the corrole layers were assessed by XPS using a standard dual anode X-ray tube with Mg and Al K_α lines. However, XPS was not performed prior to TPD measurements to avoid possible effects of radiation damage.

Density Functional Theory (DFT). The calculations were performed within the Vienna *ab initio* Simulation Package (VASP)[51] to optimize the microscopic structures of the investigated systems. Exchange and correlation interactions have been modeled by employing the gradient-corrected PW91 functional[52] complemented with a dispersion correction (DFT-D),[53] which provides accurate adsorption energies and structures for surface-adsorbed molecules at virtually low computational costs.[54−59] The electron−ion interaction was described by using pseudopotentials and the projector-augmented wave (PAW) method.[60] As a basis set, we used plane waves with kinetic energies up to 400 eV. The Ag(111) surface was modeled by periodically repeated slabs of four Ag layers separated by a vacuum of a thickness of 2.5 nm, corresponding to 12 Ag layers. The topmost two layers and all atoms of the molecule were allowed to relax freely, whereas the atoms in the two lowest layers were kept frozen at ideal bulk positions. The structural relaxations were performed with convergence criteria of 0.3 eV/nm and 1×10^{-5} eV for forces and total energies, respectively, whereby for Brillouin zone sampling, the gamma-point approximation turns out to be sufficient. XPS spectra are calculated using a delta-scf approach, which for light elements such as nitrogen has been shown to give highly accurate core-level shifts.[61−63] To model the 1s core holes of the C and N species, multiprojector (GI-)PAW pseudopotentials with a corresponding occupation of the inner shells have been generated and applied by using Quantum ESPRESSO package[64] for the VASP-relaxed molecular structures. The resulting CLS are superimposed and convoluted by assuming a line width of 0.7 eV.

ASSOCIATED CONTENT

Supporting Information

The Supporting Information is available free of charge on the ACS Publications website at DOI: 10.1021/acsnano.7b00766.

Figures S1−S6 include the peak analysis of the XPS C 1s and XPS N 1s (performed at 330, 430, 550, and 700 K); experimental STM images of corrole monolayer on Ag(111) annealed to 460 K; Kondo signal at 460 K; comparison of the experimental high-temperature (550 and 700 K) C 1s XPS signatures and the model-based simulations (PDF)

AUTHOR INFORMATION

Corresponding Authors

*E-mail: uwe.gerstmann@upb.de.
*E-mail: eva.rauls@upb.de.
*E-mail: florian.klappenberger@tum.de.
*E-mail: wolfgang.schoefberger@jku.at.
*E-mail: stefan.muellegger@jku.at.

ORCID

Mario Waser: 0000-0002-8421-8642
Florian Klappenberger: 0000-0002-2877-6105
Wolfgang Schöfberger: 0000-0002-8055-8906

Author Contributions

⊥These authors contributed equally to this work.

Notes

The authors declare no competing financial interest.

ACKNOWLEDGMENTS

Funding provided by the Austrian Science Fund (FWF) *via* D-A-CH i958 "High-Valent Metal Tetrapyrroles for Surface-Supported Catalysis" and "Oxygen and Hydrogen Evolution Triggered by Surface-Supported Catalysts" P28167-N34, the European Union *via* ERC advanced grant MolArt (grant 247299), the German Research Foundation (DFG) *via* KL 2294/3-1, FOR-1405, GRK 1464, and the Munich-Center for Advanced Photonics (MAP) is gratefully acknowledged. Computational resources were allocated at the HLRS Stuttgart and the Paderborn Center for Parallel Computing (PC^2). We also thank the Helmholtz-Zentrum, Berlin, for the allocation of synchrotron radiation beamtime and for financial support. We thank Peter Feulner for his support in setting up the XPS-TPD chamber in Bessy II (Berlin) and in our on-campus laboratory (TUM-Garching) and for fruitful discussion during the measurements. The NMR spectrometers were acquired in collaboration with the University of South Bohemia (CZ) with financial support from the European Union through the EFRE INTERREG IV ETC-AT-CZ program (project M00146, "RERI-uasb").

REFERENCES

(1) Collman, J. P.; Devaraj, N. K.; Decréau, R. A.; Yang, Y.; Yan, Y.-L.; Ebina, W.; Eberspacher, T. A.; Chidsey, C. E. D. A Cytochrome C Oxidase Model Catalyzes Oxygen to Water Reduction under Rate-Limiting Electron Flux. *Science* **2007**, *315*, 1565.

(2) Hulsken, B.; van Hameren, R.; Gerritsen, J. W.; Khoury, T.; Thordarson, P.; Crossley, M. J.; Rowan, A. E.; Nolte, R. J. M.; Elemans, JohanneJ. A. A. W.; Speller, S. Real-Time Single-Molecule Imaging of Oxidation Catalysis at a Liquid−Solid Interface. *Nat. Nanotechnol.* **2007**, *2*, 285−289.

(3) Xue, T.; Jiang, S.; Qu, Y.; Su, Q.; Cheng, R.; Dubin, S.; Chiu, C.-Y.; Kaner, R.; Huang, Y.; Duan, X. Graphene-Supported Hemin as a Highly Active Biomimetic Oxidation Catalyst. *Angew. Chem., Int. Ed.* **2012**, *51*, 3822−3825.

(4) Jahan, M.; Bao, Q.; Loh, K. P. Electrocatalytically Active Graphene−Porphyrin MOF Composite for Oxygen Reduction Reaction. *J. Am. Chem. Soc.* **2012**, *134*, 6707−6713.

(5) Sedona, F.; Di Marino, M.; Forrer, D.; Vittadini, A.; Casarin, M.; Cossaro, A.; Floreano, L.; Verdini, A.; Sambi, M. Tuning the Catalytic Activity of Ag(110)-Supported Fe Phthalocyanine in the Oxygen Reduction Reaction. *Nat. Mater.* **2012**, *11*, 970−977.

(6) Den Boer, D.; Li, M.; Habets, T.; Iavicoli, P.; Rowan, A. E.; Nolte, R. J. M.; Speller, S.; Amabilino, D. B.; de Feyter, S.; Elemans, JohanneJ. A. A. W. Detection of Different Oxidation States of Individual Manganese Porphyrins During Their Reaction with Oxygen at a Solid/Liquid Interface. *Nat. Chem.* **2013**, *5*, 621−627.

DOI: 10.1021/acsnano.7b00766
ACS Nano 2017, 11, 3383−3391

(7) Auwärter, W.; Écija, D.; Klappenberger, F.; Barth, J. V. Porphyrins at Interfaces. *Nat. Chem.* **2015**, *7*, 105−120.
(8) Gottfried, J. M. Surface Chemistry of Porphyrins and Phthalocyanines. *Surf. Sci. Rep.* **2015**, *70*, 259−379.
(9) Gourdon, A. On-Surface Covalent Coupling in Ultrahigh Vacuum. *Angew. Chem., Int. Ed.* **2008**, *47*, 6950−6953.
(10) Klappenberger, F.; Zhang, Y.-Q.; Björk, J.; Klyatskaya, S.; Ruben, M.; Barth, J. V. On-Surface Synthesis of Carbon-Based Scaffolds and Nanomaterials Using Terminal Alkynes. *Acc. Chem. Res.* **2015**, *48*, 2140−2150.
(11) Dong, L.; Liu, P. N.; Lin, N. Surface-Activated Coupling Reactions Confined on a Surface. *Acc. Chem. Res.* **2015**, *48*, 2765−2774.
(12) Fan, Q.; Gottfried, J. M.; Zhu, J. Surface-Catalyzed C−C Covalent Coupling Strategies Toward the Synthesis of Low-Dimensional Carbon-Based Nanostructures. *Acc. Chem. Res.* **2015**, *48*, 2484−2494.
(13) Talirz, L.; Ruffieux, P.; Fasel, R. On-Surface Synthesis of Atomically Precise Graphene Nanoribbons. *Adv. Mater.* **2016**, *28*, 6222−6231.
(14) Lipton-Duffin, J. A.; Ivasenko, O.; Perepichka, D. F.; Rosei, F. Synthesis of Polyphenylene Molecular Wires by Surface-Confined Polymerization. *Small* **2009**, *5*, 592−597.
(15) Treier, M.; Richardson, N. V.; Fasel, R. Fabrication of Surface-Supported Low-Dimensional Polyimide Networks. *J. Am. Chem. Soc.* **2008**, *130*, 14054−14055.
(16) Treier, M.; Fasel, R.; Champness, N. R.; Argent, S.; Richardson, N. V. Molecular Imaging of Polyimide Formation. *Phys. Chem. Chem. Phys.* **2009**, *11*, 1209.
(17) Grill, L.; R, F.; Al, B. M. K.; Vadgama, P.; Crump, P.; Wilson, S. Functionalized Molecules Studied by STM: Motion, Switching and Reactivity. *J. Phys.: Condens. Matter* **2008**, *20*, 053001.
(18) In't Veld, M.; Iavicoli, P.; Haq, S.; Amabilino, D. B.; Raval, R. Unique Intermolecular Reaction of Simple Porphyrins at a Metal Surface Gives Covalent Nanostructures. *Chem. Commun.* **2008**, *0*, 1536.
(19) Treier, M.; Pignedoli, C. A.; Laino, T.; Rieger, R.; Müllen, K.; Passerone, D.; Fasel, R. Surface-Assisted Cyclodehydrogenation Provides a Synthetic Route Towards Easily Processable and Chemically Tailored Nanographenes. *Nat. Chem.* **2011**, *3*, 61−67.
(20) Matena, M.; Riehm, T.; Stöhr, M.; Jung, T. A.; Gade, L. H. Transforming Surface Coordination Polymers into Covalent Surface Polymers: Linked Polycondensed Aromatics through Oligomerization of N-Heterocyclic Carbene Intermediates. *Angew. Chem., Int. Ed.* **2008**, *47*, 2414−2417.
(21) Weigelt, S.; Busse, C.; Bombis, C.; Knudsen, M. M.; Gothelf, K. V.; Lægsgaard, E.; Besenbacher, F.; Linderoth, T. R. Surface Synthesis of 2D Branched Polymer Nanostructures. *Angew. Chem., Int. Ed.* **2008**, *47*, 4406−4410.
(22) Malacria, M. Selective Preparation of Complex Polycyclic Molecules from Acyclic Precursors *via* Radical Mediated- or Transition Metal-Catalyzed Cascade Reactions. *Chem. Rev.* **1996**, *96*, 289−306.
(23) McCarroll, A. J.; Walton, J. C. Programming Organic Molecules: Design and Management of Organic Syntheses Through Free-Radical Cascade Processes. *Angew. Chem., Int. Ed.* **2001**, *40*, 2224−2248.
(24) Wille, U. Radical Cascades Initiated by Intermolecular Radical Addition to Alkynes and Related Triple Bond Systems. *Chem. Rev.* **2013**, *113*, 813−853.
(25) Tietze, L. F.; Brasche, G.; Gericke, K. M. Radical Domino Reactions. *Domino Reactions in Organic Synthesis*; Wiley-VCH Verlag GmbH & Co. KGaA: Weinheim, Germany, 2006; pp 219−279.
(26) Forbes, M. D. E.; Lebedeva, N. V. Acrylic Polymer Radicals: Structural Characterization and Dynamics. In *Carbon-Centered Free Radicals and Radical Cations*; Forbes, M. D. E., Ed.; John Wiley & Sons, Inc: Hoboken, NJ, 2010; pp 325−357.
(27) *Science of Synthesis Reference Library 1: Applications of Domino Transformations in Organic Synthesis*; Snyder, S. A., Ed.; Georg Thieme Verlag KG: Stuttgart, Germany, 2016.
(28) Trost, B. M. The Atom Economy-a Search for Synthetic Efficiency. *Science* **1991**, *254*, 1471−1477.
(29) Perchyonok, T.; Lykakis, I. N.; Postigo, A. *Streamlining Free Radical Green Chemistry*; The Royal Society of Chemistry: London, 2012.
(30) König, M.; Faschinger, F.; Reith, L. M.; Schöfberger, W. The Evolution of Corrole Synthesis - From Simple One-Pot Strategies to Sophisticated ABC-Corroles. *J. Porphyrins Phthalocyanines* **2016**, *20*, 96−107.
(31) Aldahhak, H.; Paszkiewicz, M.; Allegretti, F.; Duncan, D. A.; Tebi, S.; Deimel, P. S.; Casado Aguilar, P.; Zhang, Y.-Q.; Papageorgiou, A. C.; Koch, R.; Barth, J. V.; Schmidt, W. G.; Müllegger, S.; Schöfberger, W.; Klappenberger, F.; Rauls, E.; Gerstmann, U. X-ray Spectroscopy of Thin Film Free-Base Corroles: A Combined Theoretical and Experimental Characterization. *J. Phys. Chem. C* **2017**, *121*, 2192−2200.
(32) Tebi, S.; Aldahhak, H.; Serrano, G.; Schöfberger, W.; Rauls, E.; Schmidt, W. G.; Koch, R.; Müllegger, S. Manipulation Resolves Non-Trivial Structure of Corrole Monolayer on Ag(111). *Nanotechnology* **2016**, *27*, 025704.
(33) Rashidi, M.; Müllegger, S.; Roithner, M.; Schöfberger, W.; Koch, R. Spectroscopic Scanning Tunneling Microscopy Studies of Single Surface-Supported Free-Base Corroles. *J. Am. Chem. Soc.* **2012**, *134*, 91−94.
(34) Schöfberger, W.; Faschinger, F.; Chattopadhyay, S.; Bhakta, S.; Mondal, B.; Elemans, J. A. A. W.; Müllegger, S.; Tebi, S.; Koch, R.; Klappenberger, F.; Paszkiewicz, M.; Barth, J. V.; Rauls, E.; Aldahhak, H.; Schmidt, W. G.; Dey, A. A Bifunctional Electrocatalyst for Oxygen Evolution and Oxygen Reduction Reactions in Water. *Angew. Chem., Int. Ed.* **2016**, *55*, 2350−2355.
(35) Röckert, M.; Franke, M.; Tariq, Q.; Lungerich, D.; Jux, N.; Stark, M.; Kaftan, A.; Ditze, S.; Marbach, H.; Laurin, M.; Libuda, J.; Steinrück, H.-P.; Lytken, O. Insights in Reaction Mechanistics: Isotopic Exchange during the Metalation of Deuterated Tetraphenyl-21,23D-porphyrin on Cu(111). *J. Phys. Chem. C* **2014**, *118*, 26729−26736.
(36) Montoya, A.; Schlunke, A.; Haynes, B. S. Reaction of Hydrogen with Ag(111): Binding states, Minimum Energy Paths, and Kinetics. *J. Phys. Chem. B* **2006**, *110*, 17145−17154.
(37) Madhavan, V.; Chen, W.; Jamneala, T.; Crommie, M. F.; Wingreen, N. S.; Kondo, J.; Grüner, G.; Zawadowski, A.; Yazdani, A.; Jones, B. A.; Lutz, C. P.; Eigler, D. M.; Boyce, J. B.; Slichter, C. P.; Chandrasekhar, V.; Blachly, M. A.; Giordano, N.; Riegel, D.; Gross, K. D.; Daybell, M. D.; et al. Tunneling into a Single Magnetic Atom: Spectroscopic Evidence of the Kondo Resonance. *Science* **1998**, *280*, 567−569.
(38) Li, J.; Schneider, W.-D.; Berndt, R.; Delley, B. Kondo Scattering Observed at a Single Magnetic Impurity. *Phys. Rev. Lett.* **1998**, *80*, 2893−2896.
(39) Müllegger, S.; Rashidi, M.; Fattinger, M.; Koch, R. Surface-Supported Hydrocarbon π Radicals show Kondo Behavior. *J. Phys. Chem. C* **2013**, *117*, 5718−5721.
(40) Schweyen, P.; Brandhorst, K.; Wicht, R.; Wolfram, B.; Bröring, M. The Corrole Radical. *Angew. Chem., Int. Ed.* **2015**, *54*, 8213−8216.
(41) Hewson, A. C. *The Kondo Problem to Heavy Fermions*; Cambridge University Press: Cambridge, U.K., 1993.
(42) Fano, U. Effects of Configuration Interaction on Intensities and Phase Shifts. *Phys. Rev.* **1961**, *124*, 1866−1878.
(43) Wu, F.; Liu, J.; Mishra, P.; Komeda, T.; Mack, J.; Chang, Y.; Kobayashi, N.; Shen, Z. Modulation of the Molecular Spintronic Properties of Adsorbed Copper Corroles. *Nat. Commun.* **2015**, *6*, 7547.
(44) Kuck, S.; Hoffmann, G.; Bröring, M.; Fechtel, M.; Funk, M.; Wiesendanger, R. "Naked" Iron-5,10,15-Triphenylcorrole on Cu(111): Observation of Chirality on a Surface and Manipulation of Multiple Conformational States by STM. *J. Am. Chem. Soc.* **2008**, *130*, 14072.
(45) Pacilé, D.; Papagno, M.; Fraile Rodríguez, A.; Grioni, M.; Papagno, L.; et al. Near-Edge X-Ray Absorption Fine-Structure Investigation of Graphene. *Phys. Rev. Lett.* **2008**, *101*, 66806.

DOI: 10.1021/acsnano.7b00766
ACS Nano 2017, 11, 3383−3391

(46) Gao, Y.; Hu, G.; Zhong, J.; Shi, Z.; Zhu, Y.; Su, D. S.; Wang, J.; Bao, X.; Ma, D. Nitrogen-Doped sp^2-Hybridized Carbon as a Superior Catalyst for Selective Oxidation. *Angew. Chem., Int. Ed.* **2013**, *52*, 2109−2113.
(47) Diller, K.; Papageorgiou, A. C.; Klappenberger, F.; Allegretti, F.; Barth, J. V.; Auwärter, W. In Vacuo Interfacial Tetrapyrrole Metallation. *Chem. Soc. Rev.* **2016**, *45*, 1629−1656.
(48) Reith, L. M.; Stiftinger, M.; Monkowius, U.; Knör, G.; Schoefberger, W. Synthesis and Characterization of a Stable Bismuth(III) A_3-Corrole. *Inorg. Chem.* **2011**, *50*, 6788.
(49) Berndt, R.; Li, J.; Schneider, W. D.; Crampin, S. Surface-State Linewidth from Scanning Tunnelling Spectroscopy. *Appl. Phys. A: Mater. Sci. Process.* **1999**, *69*, 503−506.
(50) Horcas, I.; Fernandez, R.; Gomez-Rodriguez, J. M.; Colchero, J.; Gomez-Herrero, J.; Baro, A. M. WSXM: A Software for Scanning Probe Microscopy and a Tool for Nanotechnology. *Rev. Sci. Instrum.* **2007**, *78*, 013705.
(51) Kresse, G.; Furthmüller, J. Efficiency of *Ab-Initio* Total Energy Calculations for Metals and Semiconductors using a Plane-Wave Basis Set. *Comput. Mater. Sci.* **1996**, *6*, 15−50.
(52) Perdew, J. P.; Chevary, J. A.; Vosko, S. H.; Jackson, K. A.; Pederson, M. R.; Singh, D. J.; Fiolhais, C. Atoms, Molecules, Solids, and Surfaces: Applications of the Generalized Gradient Approximation for Exchange and Correlation. *Phys. Rev. B: Condens. Matter Mater. Phys.* **1992**, *46*, 6671−6687.
(53) Ortmann, F.; Bechstedt, F.; Schmidt, W. G. Semiempirical Van der Waals Correction to the Density Functional Description of Solids and Molecular Structures. *Phys. Rev. B: Condens. Matter Mater. Phys.* **2006**, *73*, 205101.
(54) McNellis, E. R.; Meyer, J.; Reuter, K. Azobenzene at Coinage Metal surfaces: Role of Dispersive Van der Waals Interactions. *Phys. Rev. B: Condens. Matter Mater. Phys.* **2009**, *80*, 205414.
(55) Thierfelder, C.; Witte, M.; Blankenburg, S.; Rauls, E.; Schmidt, W. G. Methane Adsorption on Graphene from First Principles Including Dispersion Interaction. *Surf. Sci.* **2011**, *605*, 746−749.
(56) Aldahhak, H.; Schmidt, W. G.; Rauls, E. Adsorption of PTCDA on NaCl(100) and KCl(100). *Surf. Sci.* **2013**, *617*, 242−248.
(57) Guo, Q.; Paulheim, A.; Sokolowski, M.; Aldahhak, H.; Rauls, E.; Schmidt, W. G. Adsorption of PTCDA on Terraces and at Steps Sites of the KCl(100) Surface. *J. Phys. Chem. C* **2014**, *118*, 29911−29918.
(58) Aldahhak, H.; Schmidt, W. G.; Rauls, E. Single PTCDA Molecules on Planar and Stepped KCl and NaCl(100) Surfaces. *Surf. Sci.* **2015**, *641*, 278−281.
(59) Aldahhak, H.; Matencio, S.; Barrena, E.; Ocal, C.; Schmidt, W. G.; Rauls, E. Structure Formation in Diindenoperylene Thin Films on Copper(111). *Phys. Chem. Chem. Phys.* **2015**, *17*, 8776−8783.
(60) Kresse, G. From Ultrasoft Pseudopotentials to the Projector Augmented-Wave Method. *Phys. Rev. B: Condens. Matter Mater. Phys.* **1999**, *59*, 1758−1775.
(61) Rignanese, G. M.; Pasquarello, A. Nitrogen Bonding Configurations at Nitrided Si(001) Surfaces and Si(001) - SiO_2 Interfaces: A First-Principles Study of Core-Level Shifts. *Phys. Rev. B: Condens. Matter Mater. Phys.* **2001**, *63*, 75307.
(62) Rignanese, G. M.; Pasquarello, A. Nitrogen 1s Core-Level Shifts at the NH_3 Saturated Si(100)-2 × 1 Surface: A First-Principles Study. *Surf. Sci.* **2001**, *490*, L614−L618.
(63) García-Gil, S.; García, A.; Ordejón, P. Calculation of Core Level Shifts within DFT using Pseudopotentials and Localized Basis Sets. *Eur. Phys. J. B* **2012**, *85*, 239.
(64) Giannozzi, P.; Baroni, S.; Bonini, N.; Calandra, M.; Car, R.; Cavazzoni, C.; Ceresoli, D.; Chiarotti, G. L.; Cococcioni, M.; Dabo, I.; Dal Corso, A.; de Gironcoli, S.; Fabris, S.; Fratesi, G.; Gebauer, R.; Gerstmann, U.; Gougoussis, C.; Kokalj, A.; Lazzeri, M.; Martin-Samos, L.; et al. Quantum Espresso: Amodular and Open-Source Software Project for Quantum Simulations of Materials. *J. Phys.: Condens. Matter* **2009**, *21*, 395502.

DOI: 10.1021/acsnano.7b00766
ACS Nano 2017, 11, 3383−3391